Research Article | Vol. 9, No. 3 | 1 Mar 2018 | BIOMEDICAL OPTICS EXPRESS 1283
Biomedical Optics EXPRESS

Manipulating the mitochondria activity in human hepatic cell line Huh7 by low-power laser irradiation

ANNA LYNNYK,[1] MARIIA LUNOVA,[1,2] MILAN JIRSA,[2] DARIA EGOROVA,[3] ANDREI KULIKOV,[3] ŠÁRKA KUBINOVÁ,[1,4] OLEG LUNOV,[1,*] AND ALEXANDR DEJNEKA[1]

[1]*Institute of Physics of the Czech Academy of Sciences, Prague, 18221, Czech Republic*
[2]*Institute for Clinical & Experimental Medicine (IKEM), Prague, 14021, Czech Republic*
[3]*ITMO University, St. Petersburg, 197101, Russia*
[4]*Institute of Experimental Medicine of the Czech Academy of Sciences, Prague, 14220, Czech Republic*
**lunov@fzu.cz*

Abstract: Low-power laser irradiation of red light has been recognized as a promising tool across a vast variety of biomedical applications. However, deep understanding of the molecular mechanisms behind laser-induced cellular effects remains a significant challenge. Here, we investigated mechanisms involved in the death process in human hepatic cell line Huh7 at a laser irradiation. We decoupled distinct cell death pathways targeted by laser irradiations of different powers. Our data demonstrate that high dose laser irradiation exhibited the highest levels of total reactive oxygen species production, leading to cyclophilin D-related necrosis via the mitochondrial permeability transition. On the contrary, low dose laser irradiation resulted in the nuclear accumulation of superoxide and apoptosis execution. Our findings offer a novel insight into laser-induced cellular responses, and reveal distinct cell death pathways triggered by laser irradiation. The observed link between mitochondria depolarization and triggering ROS could be a fundamental phenomenon in laser-induced cellular responses.

OCIS codes: (170.0170) Medical optics and biotechnology; (170.1420) Biology; (170.1530) Cell analysis.

References and links

1. R. R. Anderson, "Lasers for dermatology and skin biology," J. Invest. Dermatol. **133**(E1), E21–E23 (2013).
2. N. Shirasu, S. O. Nam, and M. Kuroki, "Tumor-targeted photodynamic therapy," Anticancer Res. **33**(7), 2823–2831 (2013).
3. H. Chung, T. Dai, S. K. Sharma, Y. Y. Huang, J. D. Carroll, and M. R. Hamblin, "The nuts and bolts of low-level laser (light) therapy," Ann. Biomed. Eng. **40**(2), 516–533 (2012).
4. R. S. Stern, "Psoralen and ultraviolet a light therapy for psoriasis," N. Engl. J. Med. **357**(7), 682–690 (2007).
5. H. K. Soong and J. B. Malta, "Femtosecond lasers in ophthalmology," Am. J. Ophthalmol. **147**(2), 189–197.e2 (2009).
6. R. T. Chow, M. I. Johnson, R. A. Lopes-Martins, and J. M. Bjordal, "Efficacy of low-level laser therapy in the management of neck pain: A systematic review and meta-analysis of randomised placebo or active-treatment controlled trials," Lancet **374**(9705), 1897–1908 (2009).
7. D. Yang, W. Yi, E. Wang, and M. Wang, "Effects of light-emitting diode irradiation on the osteogenesis of human umbilical cord mesenchymal stem cells in vitro," Sci. Rep. **6**(1), 37370 (2016).
8. W. K. Ong, H. F. Chen, C. T. Tsai, Y. J. Fu, Y. S. Wong, D. J. Yen, T. H. Chang, H. D. Huang, O. K. Lee, S. Chien, and J. H. Ho, "The activation of directional stem cell motility by green light-emitting diode irradiation," Biomaterials **34**(8), 1911–1920 (2013).
9. S. Wu, D. Xing, X. Gao, and W. R. Chen, "High fluence low-power laser irradiation induces mitochondrial permeability transition mediated by reactive oxygen species," J. Cell. Physiol. **218**(3), 603–611 (2009).
10. I. Khan, E. Tang, and P. Arany, "Molecular pathway of near-infrared laser phototoxicity involves atf-4 orchestrated er stress," Sci. Rep. **5**(1), 10581 (2015).
11. H. T. Whelan, E. V. Buchmann, A. Dhokalia, M. P. Kane, N. T. Whelan, M. T. Wong-Riley, J. T. Eells, L. J. Gould, R. Hammamieh, R. Das, and M. Jett, "Effect of nasa light-emitting diode irradiation on molecular changes for wound healing in diabetic mice," J. Clin. Laser Med. Surg. **21**(2), 67–74 (2003).

#314823 https://doi.org/10.1364/BOE.9.001283
Journal © 2018 Received 6 Dec 2017; revised 5 Feb 2018; accepted 11 Feb 2018; published 21 Feb 2018

Biomedical Optics EXPRESS

12. P. R. Arany, A. Cho, T. D. Hunt, G. Sidhu, K. Shin, E. Hahm, G. X. Huang, J. Weaver, A. C. Chen, B. L. Padwa, M. R. Hamblin, M. H. Barcellos-Hoff, A. B. Kulkarni, and D. J Mooney, "Photoactivation of endogenous latent transforming growth factor-β1 directs dental stem cell differentiation for regeneration," Sci. Transl. Med. **6**(238), 238ra69 (2014).
13. J. T. Eells, M. M. Henry, P. Summerfelt, M. T. Wong-Riley, E. V. Buchmann, M. Kane, N. T. Whelan, and H. T. Whelan, "Therapeutic photobiomodulation for methanol-induced retinal toxicity," Proc. Natl. Acad. Sci. U.S.A. **100**(6), 3439–3444 (2003).
14. L. Brosseau, V. Robinson, G. Wells, R. Debie, A. Gam, K. Harman, M. Morin, B. Shea, and P. Tugwell, "Low level laser therapy (classes i, ii and iii) for treating rheumatoid arthritis," Cochrane Database Syst. Rev. **4**, CD002049 (2005).
15. Z. Huang, J. Ma, J. Chen, B. Shen, F. Pei, and V. B. Kraus, "The effectiveness of low-level laser therapy for nonspecific chronic low back pain: A systematic review and meta-analysis," Arthritis Res. Ther. **17**(1), 360 (2015).
16. R. Yousefi-Nooraie, E. Schonstein, K. Heidari, A. Rashidian, V. Pennick, M. Akbari-Kamrani, S. Irani, B. Shakiba, S. A. Mortaz Hejri, S. O. Mortaz Hejri, and A. Jonaidi, "Low level laser therapy for nonspecific low-back pain," Cochrane Database Syst. Rev. **2**, CD005107 (2008).
17. Y. Y. Huang, A. C. Chen, J. D. Carroll, and M. R. Hamblin, "Biphasic dose response in low level light therapy," Dose Response **7**(4), 358–383 (2009).
18. Y. Y. Huang, S. K. Sharma, J. Carroll, and M. R. Hamblin, "Biphasic dose response in low level light therapy - an update," Dose Response **9**(4), 602–618 (2011).
19. T. Karu, "Photobiology of low-power laser effects," Health Phys. **56**(5), 691–704 (1989).
20. S. Wu, D. Xing, F. Wang, T. Chen, and W. R. Chen, "Mechanistic study of apoptosis induced by high-fluence low-power laser irradiation using fluorescence imaging techniques," J. Biomed. Opt. **12**(6), 064015 (2007).
21. R. A. Vacca, L. Moro, V. A. Petragallo, M. Greco, F. Fontana, and S. Passarella, "The irradiation of hepatocytes with he-ne laser causes an increase of cytosolic free calcium concentration and an increase of cell membrane potential, correlated with it, both increases taking place in an oscillatory manner," Biochem. Mol. Biol. Int. **43**(5), 1005–1014 (1997).
22. M. Greco, R. A. Vacca, L. Moro, E. Perlino, V. A. Petragallo, E. Marra, and S. Passarella, "Helium-neon laser irradiation of hepatocytes can trigger increase of the mitochondrial membrane potential and can stimulate c-fos expression in a Ca2+-dependent manner," Lasers Surg. Med. **29**(5), 433–441 (2001).
23. A. C. Chen, P. R. Arany, Y. Y. Huang, E. M. Tomkinson, S. K. Sharma, G. B. Kharkwal, T. Saleem, D. Mooney, F. E. Yull, T. S. Blackwell, and M. R. Hamblin, "Low-level laser therapy activates nf-kb via generation of reactive oxygen species in mouse embryonic fibroblasts," PLoS One **6**(7), e22453 (2011).
24. G. Mariño, M. Niso-Santano, E. H. Baehrecke, and G. Kroemer, "Self-consumption: The interplay of autophagy and apoptosis," Nat. Rev. Mol. Cell Biol. **15**(2), 81–94 (2014).
25. W. Fiers, R. Beyaert, W. Declercq, and P. Vandenabeele, "More than one way to die: Apoptosis, necrosis and reactive oxygen damage," Oncogene **18**(54), 7719–7730 (1999).
26. T. Vanden Berghe, W. J. Kaiser, M. J. M. Bertrand, and P. Vandenabeele, "Molecular crosstalk between apoptosis, necroptosis, and survival signaling," Mol. Cell. Oncol. **2**(4), e975093 (2015).
27. V. Nikoletopoulou, M. Markaki, K. Palikaras, and N. Tavernarakis, "Crosstalk between apoptosis, necrosis and autophagy," Biochim. Biophys. Acta **1833**(12), 3448–3459 (2013).
28. K. S. Lim, S. W. Harun, H. Arof, and H. Ahmad, "Fabrication and applications of microfiber," in *Selected Topics on Optical Fiber Technology*, Chapter 17 (Intech, 2012), pp. 473–508.
29. N. G. Papadopoulos, G. V. Dedoussis, G. Spanakos, A. D. Gritzapis, C. N. Baxevanis, and M. Papamichail, "An improved fluorescence assay for the determination of lymphocyte-mediated cytotoxicity using flow cytometry," J. Immunol. Methods **177**(1-2), 101–111 (1994).
30. M. A. Kang, E. Y. So, A. L. Simons, D. R. Spitz, and T. Ouchi, "DNA damage induces reactive oxygen species generation through the h2ax-nox1/rac1 pathway," Cell Death Dis. **3**, e249 (2012).
31. O. Lunov, V. Zablotskii, O. Churpita, M. Lunova, M. Jirsa, A. Dejneka, and Š. Kubinová, "Chemically different non-thermal plasmas target distinct cell death pathways," Sci. Rep. **7**(1), 600 (2017).
32. O. Lunov, V. Zablotskii, O. Churpita, A. Jäger, L. Polívka, E. Syková, A. Dejneka, and Š. Kubinová, "The interplay between biological and physical scenarios of bacterial death induced by non-thermal plasma," Biomaterials **82**, 71–83 (2016).
33. O. Lunov, V. Zablotskii, O. Churpita, E. Chánová, E. Syková, A. Dejneka, and S. Kubinová, "Cell death induced by ozone and various non-thermal plasmas: Therapeutic perspectives and limitations," Sci. Rep. **4**(1), 7129 (2015).
34. H. Wang and J. A. Joseph, "Quantifying cellular oxidative stress by dichlorofluorescein assay using microplate reader," Free Radic. Biol. Med. **27**(5-6), 612–616 (1999).
35. O. Gavet and J. Pines, "Progressive activation of cyclinb1-cdk1 coordinates entry to mitosis," Dev. Cell **18**(4), 533–543 (2010).
36. S. T. Smiley, M. Reers, C. Mottola-Hartshorn, M. Lin, A. Chen, T. W. Smith, G. D. Steele, Jr., and L. B. Chen, "Intracellular heterogeneity in mitochondrial membrane potentials revealed by a J-aggregate-forming lipophilic cation jc-1," Proc. Natl. Acad. Sci. U.S.A. **88**(9), 3671–3675 (1991).

Biomedical Optics EXPRESS

37. T. Zuliani, R. Duval, C. Jayat, S. Schnébert, P. André, M. Dumas, and M. H. Ratinaud, "Sensitive and reliable jc-1 and toto-3 double staining to assess mitochondrial transmembrane potential and plasma membrane Integrity: interest for cell death investigations," Cytometry A **54A**(2), 100–108 (2003).
38. M. Lunova, A. Prokhorov, M. Jirsa, M. Hof, A. Olżyńska, P. Jurkiewicz, Š. Kubinová, O. Lunov, and A. Dejneka, "Nanoparticle core stability and surface functionalization drive the mtor signaling pathway in hepatocellular cell lines," Sci. Rep. **7**(1), 16049 (2017).
39. S. B. Goncalves, J. F. Ribeiro, A. F. Silva, R. M. Costa, and J. H. Correia, "Design and manufacturing challenges of optogenetic neural interfaces: A review," J. Neural Eng. **14**(4), 041001 (2017).
40. O. Yizhar, L. E. Fenno, T. J. Davidson, M. Mogri, and K. Deisseroth, "Optogenetics in neural systems," Neuron **71**(1), 9–34 (2011).
41. T. A. Henderson and L. D. Morries, "Near-infrared photonic energy penetration: Can infrared phototherapy effectively reach the human brain?" Neuropsychiatr. Dis. Treat. **11**, 2191–2208 (2015).
42. M. L. Denton, M. S. Foltz, L. E. Estlack, D. J. Stolarski, G. D. Noojin, R. J. Thomas, D. Eikum, and B. A. Rockwell, "Damage thresholds for exposure to nir and blue lasers in an in vitro rpe cell system," Invest. Ophthalmol. Vis. Sci. **47**(7), 3065–3073 (2006).
43. P. S. Yarmolenko, E. J. Moon, C. Landon, A. Manzoor, D. W. Hochman, B. L. Viglianti, and M. W. Dewhirst, "Thresholds for thermal damage to normal tissues: An update," Int. J. Hyperthermia **27**(4), 320–343 (2011).
44. J. Shen, C. Chui, and X. Tao, "Luminous fabric devices for wearable low-level light therapy," Biomed. Opt. Express **4**(12), 2925–2937 (2013).
45. M. Weil, M. D. Jacobson, H. S. Coles, T. J. Davies, R. L. Gardner, K. D. Raff, and M. C. Raff, "Constitutive expression of the machinery for programmed cell death," J. Cell Biol. **133**(5), 1053–1059 (1996).
46. K. J. Henle and R. L. Warters, "Heat protection by glycerol in vitro," Cancer Res. **42**(6), 2171–2176 (1982).
47. J. F. Pittet, H. Lee, M. Pespeni, A. O'Mahony, J. Roux, and W. J. Welch, "Stress-induced inhibition of the NF-kappaB signaling pathway results from the insolubilization of the ikappab kinase complex following its dissociation from heat shock protein 90," J. Immunol. **174**(1), 384–394 (2005).
48. N. N. Danial and S. J. Korsmeyer, "Cell death: Critical control points," Cell **116**(2), 205–219 (2004).
49. M. Di Carlo, D. Giacomazza, P. Picone, D. Nuzzo, and P. L. San Biagio, "Are oxidative stress and mitochondrial dysfunction the key players in the neurodegenerative diseases?" Free Radic. Res. **46**(11), 1327–1338 (2012).
50. M. T. Lin and M. F. Beal, "Mitochondrial dysfunction and oxidative stress in neurodegenerative diseases," Nature **443**(7113), 787–795 (2006).
51. G. Kroemer and J. C. Reed, "Mitochondrial control of cell death," Nat. Med. **6**(5), 513–519 (2000).
52. J. D. Ly, D. R. Grubb, and A. Lawen, "The mitochondrial membrane potential (delta psi m) in apoptosis; an update," Apoptosis **8**(2), 115–128 (2003).
53. R. Matthes, C. Bender, R. Schlüter, I. Koban, R. Bussiahn, S. Reuter, J. Lademann, K. D. Weltmann, and A. Kramer, "Antimicrobial efficacy of two surface barrier discharges with air plasma against in vitro biofilms," PLoS One **8**(7), e70462 (2013).
54. S. T. Smiley, M. Reers, C. Mottola-Hartshorn, M. Lin, A. Chen, T. W. Smith, G. D. Steele, Jr., and L. B. Chen, "Intracellular heterogeneity in mitochondrial membrane potentials revealed by a j-aggregate-forming lipophilic cation jc-1," Proc. Natl. Acad. Sci. U.S.A. **88**(9), 3671–3675 (1991).
55. S. J. Martin, C. P. Reutelingsperger, A. J. McGahon, J. A. Rader, R. C. van Schie, D. M. LaFace, and D. R. Green, "Early redistribution of plasma membrane phosphatidylserine is a general feature of apoptosis regardless of the initiating stimulus: inhibition by overexpression of bcl-2 and abl," J. Exp. Med. **182**(5), 1545–1556 (1995).
56. J. B. Hoek, A. Cahill, and J. G. Pastorino, "Alcohol and mitochondria: A dysfunctional relationship," Gastroenterology **122**(7), 2049–2063 (2002).
57. A. Linkermann and D. R. Green, "Necroptosis," N. Engl. J. Med. **370**(5), 455–465 (2014).
58. G. Mariño, M. Niso-Santano, E. H. Baehrecke, and G. Kroemer, "Self-consumption: The interplay of autophagy and apoptosis," Nat. Rev. Mol. Cell Biol. **15**(2), 81–94 (2014).
59. A. Degterev, Z. Huang, M. Boyce, Y. Li, P. Jagtap, N. Mizushima, G. D. Cuny, T. J. Mitchison, M. A. Moskowitz, and J. Yuan, "Chemical inhibitor of nonapoptotic cell death with therapeutic potential for ischemic brain injury," Nat. Chem. Biol. **1**(2), 112–119 (2005).
60. E. Panieri, V. Gogvadze, E. Norberg, R. Venkatesh, S. Orrenius, and B. Zhivotovsky, "Reactive oxygen species generated in different compartments induce cell death, survival, or senescence," Free Radic. Biol. Med. **57**, 176–187 (2013).
61. A. Valencia and J. Morán, "Reactive oxygen species induce different cell death mechanisms in cultured neurons," Free Radic. Biol. Med. **36**(9), 1112–1125 (2004).
62. H. A. Woo, S. H. Yim, D. H. Shin, D. Kang, D. Y. Yu, and S. G. Rhee, "Inactivation of peroxiredoxin i by phosphorylation allows localized h2o2 accumulation for cell signaling," Cell **140**(4), 517–528 (2010).
63. H. C. Birnboim and M. Kanabus-Kaminska, "The production of DNA strand breaks in human leukocytes by superoxide anion may involve a metabolic process," Proc. Natl. Acad. Sci. U.S.A. **82**(20), 6820–6824 (1985).
64. W. P. Roos, A. D. Thomas, and B. Kaina, "DNA damage and the balance between survival and death in cancer biology," Nat. Rev. Cancer **16**(1), 20–33 (2016).
65. F. Wang, T. S. Chen, D. Xing, J. J. Wang, and Y. X. Wu, "Measuring dynamics of caspase-3 activity in living cells using FRET technique during apoptosis induced by high fluence low-power laser irradiation," Lasers Surg. Med. **36**(1), 2–7 (2005).

Biomedical Optics EXPRESS

66. C. C. Winterbourn, "Reconciling the chemistry and biology of reactive oxygen species," Nat. Chem. Biol. **4**(5), 278–286 (2008).
67. S. Y. Ryu, P. M. Peixoto, O. Teijido, L. M. Dejean, and K. W. Kinnally, "Role of mitochondrial ion channels in cell death," Biofactors **36**(4), 255–263 (2010).
68. K. W. Kinnally, P. M. Peixoto, S. Y. Ryu, and L. M. Dejean, "Is mptp the gatekeeper for necrosis, apoptosis, or both?" Biochim. Biophys. Acta **1813**(4), 616–622 (2011).
69. S. W. Tait and D. R. Green, "Mitochondria and cell death: Outer membrane permeabilization and beyond," Nat. Rev. Mol. Cell Biol. **11**(9), 621–632 (2010).
70. H. Vakifahmetoglu-Norberg, A. T. Ouchida, and E. Norberg, "The role of mitochondria in metabolism and cell death," Biochem. Biophys. Res. Commun. **482**(3), 426–431 (2017).
71. Y. Wang, H. He, S. Wang, Y. Liu, M. Hu, Y. Cao, S. Kong, X. Wei, and C. Wang, "Photostimulation by femtosecond laser triggers restorable fragmentation in single mitochondrion," J. Biophotonics **10**(2), 286–293 (2017).
72. Y. Zhu and H. He, "Molecular response of mitochondria to a short-duration femtosecond-laser stimulation," Biomed. Opt. Express **8**(11), 4965–4973 (2017).
73. S. Wu, F. Zhou, Z. Zhang, and D. Xing, "Mitochondrial oxidative stress causes mitochondrial fragmentation via differential modulation of mitochondrial fission-fusion proteins," FEBS J. **278**(6), 941–954 (2011).
74. M. P. Murphy, "How mitochondria produce reactive oxygen species," Biochem. J. **417**(1), 1–13 (2009).
75. J. Moon, J. Yun, Y. D. Yoon, S. I. Park, Y. J. Seo, W. S. Park, H. Y. Chu, K. H. Park, M. Y. Lee, C. W. Lee, S. J. Oh, Y. S. Kwak, Y. P. Jang, and J. S. Kang, "Blue light effect on retinal pigment epithelial cells by display devices," Integr. Biol. **9**(5), 436–443 (2017).
76. T. I. Karu, L. V. Pyatibrat, S. F. Kolyakov, and N. I. Afanasyeva, "Absorption measurements of cell monolayers relevant to mechanisms of laser phototherapy: Reduction or oxidation of cytochrome c oxidase under laser radiation at 632.8 nm," Photomed. Laser Surg. **26**(6), 593–599 (2008).
77. N. Kaludercic, S. Deshwal, and F. Di Lisa, "Reactive oxygen species and redox compartmentalization," Front. Physiol. **5**, 285 (2014).

1. Introduction

Light plays a crucial role in important biological processes directly related to a human health such as: vision, vitamin-D metabolism, circadian rhythm and psychosocial state. It is not surprising that light, as a physical cue, has been found useful in different clinical applications such as phototherapy, photodynamic therapy (PDT) and skin rejuvenation [1–4]. In particular, low power red and near-infrared (NIR) lasers are gaining steadily increasing attention in a wide range of biomedical applications ranging from ophthalmology to oncology [2, 3, 5, 6]. Low-power laser irradiation with red light (600-680 nm) has been shown to modulate various biological processes, such as cell proliferation and differentiation [7], cell viability, motility [8], and cell apoptosis [9, 10]. Burst of research in this direction resulted in therapeutic applications of low power red and near-infrared light to promote wound healing, hair growth, tissue regeneration or reduce pain and inflammation termed as Low Level Light/Laser Therapy (LLLT) [3, 6, 11–13]. Although LLLT became widely used to treat a variety of ailments, it remains controversial [14–16]. These inconsistencies in the literature are not surprising. Despite that the biological effects of low power red and near-infrared (NIR) radiation have been studied for decades, its underlying biochemical mechanisms remain poorly understood. Moreover, LLLT therapy demonstrates a biphasic dose response curve, where low doses appear to have beneficial therapeutic effects while higher doses are harmful (phototoxic) [17, 18]. So far, effects of low power red and near-infrared light on biological responses and safety have not been investigated thoroughly. Furthermore, for each laser treatment, a large number of parameters must be taken into account, such as the wavelength, fluence, power density, pulse structure etc. Thus, only the knowledge of the spatiotemporal mechanisms of the laser-induced effects will enable the deliberate exploitation of cellular signaling processes. Such knowledge is crucial for the development of well-controlled laser applications to achieve a significant therapeutic benefit.

Mitochondria have been reasonably proposed as an intracellular target of red and near-infra-red light [9, 19]. Recent works showed that low-power red (633 nm) laser irradiation triggers cell apoptosis through the mitochondrial signaling pathway (mitochondria/caspase-3) [9, 20]. Up to now, only a few studies have investigated the impact of red laser irradiation on hepatocyte cell behavior [21, 22]. It has been demonstrated that red (632.8 nm) laser

Biomedical Optics EXPRESS

irradiation changes cytosolic free calcium concentration and results in changes of the mitochondrial membrane potential [21, 22]. Moreover, it has been shown that red laser light may initiate apoptosis via the induction of reactive oxygen species-mediated mitochondrial permeability transition [9]. It has also been reported that red light-induced red damage is mainly caused by the production of reactive oxygen species (ROS) in the mitochondria [3, 9, 20, 23]. Since tissues with higher energy requirement like red muscle and liver have a higher number of mitochondria, it makes liver-derived cell lines an attractive model to study laser irradiation effects on living cells. Interestingly, mitochondrial damage has been implicated in both necrotic and apoptotic cell death [24, 25]. Furthermore, it is now well established that there is a substantial molecular crosstalk between apoptosis and necrosis pathways and mitochondria play crucial role in this crosstalk [26, 27]. In this context, we explored specifically designed laser potential for remote control of mitochondria activity and triggering different signaling cascades utilizing the same laser wavelength.

2. Materials and methods

Design and characterization of the laser system

To produce uniform laser irradiation for biological applications, we utilized the system shown on Fig. 1(A). The optical circuit includes a laser diode module LDI-FP-660-20-X-3-SM04-FU-CW with a fiber output of red light at the wavelength of 655 nm. The system offers the ability to adjust the output power of laser radiation (Fig. 1(B)). As a delivery system for laser radiation, a single-mode optical fiber of the SMF-28 type (Corning, New York, US) with a reduced diameter at the output end (biconical optical taper) was connected to the laser diode through an optical socket (Fig. 1(B)). Unlike other existing methods of optical radiation delivery, a fiber taper with a waist diameter of 15 ± 5 μm allows to influence not only individual cells, but also certain regions of cells whose size exceeds the diameter of the waistband. Biconical optical tapers were produced by an apparatus for welding optical fibers Fujikura FSM-100M/P utilizing the previously published methodology [28]. Further, in order to eliminate the undesirable effects of optical radiation propagation, a protective coating of titanium dioxide (TiO_2) was formed by the ion sputtering method at the waistband of the biconical taper. After the process of spraying the protective coating, the fiber optic taper was scraped a few millimeters from the narrowest point in the waist, and the fiber end was polished on a Bare Fiber Polisher (Krell Technologies, Neptune City, NJ).

Cell culture

The human hepatocellular carcinoma cell line Huh7 obtained from the Japanese Collection of Research Bioresources (JCRB) were cultured in EMEM medium (American Type Culture Collection, ATCC) supplemented with 10% fetal calf serum (FCS) as recommended by the supplier. Cultures were kept in a humidified 5% CO_2 atmosphere at 37°C and the medium was changed twice a week.

Laser treatment

Huh7 cells were seeded in 35 mm tissue culture IBIDI μ-dishes (IBIDI, Munich, Germany) 24 h before laser irradiation. Depending on the experiment, cells were labeled either prior laser irradiation or immediately after. Positioning of optical tapers in the closest proximity to the cells was performed using an Eppendorf micromanipulator (5171, Eppendorf, Wesseling-Berzdorf, Germany) that was connected to a Nikon Diaphot 200 microscope (Nikon, Tokyo, Japan) (Fig. 1(A)). Optical tapers were sterilized with 75% ethanol prior positioning to the cells.

Biomedical Optics EXPRESS

Chemicals

The following fluorescent probes were used: Cellular ROS/Superoxide Detection Assay Kit (Abcam, Cambridge, United Kingdom) to detect the generation of ROS and superoxide; and acetoxymethylester of calcein (calcein-AM, 1 μM) and ethidium homodimer (EthD-1, 4 μM) to monitor cell viability; JC-1 (2 μM) to monitor mitochondrial membrane potential and VAD-FMK conjugated to FITC (FITC-VAD-FMK) to detect caspase-3 activation. Calcein-AM, ethidium homodimer and JC-1 probes were purchased from Thermo Fisher Scientific. Cellular ROS/Superoxide Detection Assay Kit and FITC-VAD-FMK were purchased from Abcam. To specifically investigate mitochondrial ROS, cells were loaded with MitoTracker red CM-H_2XRos (reduced form of MitoTracker red; 0.5 μM; Thermo Fisher Scientific) by incubating them for 15 min. The cell-permeant SYTO 13 green fluorescent nucleic acid stain (5 μM; Thermo Fisher Scientific) was used to label nucleus. The optimal incubation time for each probe was determined experimentally.

The following reagents were used: cyclosporin A (CsA, 10 μM) to inhibit the mitochondrial permeability transition; necrostatin-1 (Nec-1, 10 μM) as a potent and selective inhibitor of necroptosis; *N-acetyl-L-cysteine* (NAC, 5 mM) to scavenge ROS; staurosporine (STS, 2 μM) as a known inducer of apoptosis; pyocyanin (200 μM) as a known ROS inducer. Necrostatin-1, cyclosporine A and *N-acetyl-L-cysteine* were purchased from Sigma–Aldrich. Staurosporine and pyocyanin were purchased from Abcam. CellMask Deep Red purchased from Thermo Fisher Scientific was used for plasma membrane staining.

Measurement of cellular viability

Cell viability was analyzed by fluorescent live/dead cell assay kit (Thermo Fisher Scientific). This two-color fluorescence cell viability assay is based on the ability of calcein AM to be retained within live cells, inducing an intense uniform green fluorescence and EthD-1 to bind the nuclei of damaged cells, thus producing a bright red fluorescence in dead cells [29]. For timed-course analysis, Huh7 cells were seeded in 35 mm tissue culture IBIDI μ-dishes (IBIDI, Munich, Germany) 24 h before labeling. Cells were stained with calcein-AM (1 μM) and EthD-1 (4 μM) for 30 min. After labeling cells were exposed to laser light. Subsequently images were captured using Bio-Rad MRC-1024 laser scanning confocal microscope (Bio-Rad, Cambridge, MA) for 50 min with 2 min interval between images. ImageJ software (NIH) was used for image processing. Fluorescence intensity of both dyes was measured at the respective time points and was normalized to total fluorescence 30 min after dye loading. In order to confirm the validity of the live/dead staining were also treated with 10% ethanol for 10 min and subsequent imaging (data not shown).

Detection of intracellular reactive oxygen species (ROS)

ROS levels were measured using the Cellular ROS/Superoxide Detection Assay Kit (Abcam, Cambridge, United Kingdom). Cells were seeded onto 35 mm tissue culture IBIDI μ-dishes (IBIDI, Munich, Germany). After laser treatment cells were labeled with fluorescent reporter dyes, which are oxidized by ROS with high specificity, according to the manufacturer's instruction (Abcam, Cambridge, United Kingdom). For total ROS detection we used the cell permeant reagent 2',7' –dichlorofluorescein diacetate (DCFDA), a fluorogenic dye that measures hydroxyl, peroxyl and other ROS activity within the cell. Dihydroethidium (hydroethidine or DHE) was used for superoxide detection. Fluorescent images were captured using Bio-Rad MRC-1024 laser scanning confocal microscope (Bio-Rad, Cambridge, MA). Fluorescence intensity was measured using ImageJ software (NIH, Bethesda, MD). Quantification of ROS levels was done using previously published methods [30–34]. Briefly, we calculated fluorescence using the formula $[(F_{t10} - F_{t0})/F_{t0}]$, where F_{t10} is fluorescence at time 10 min (time needed for the dye to effectively label reactive oxygen species in cells) and F_{t0} – fluorescence at time 0 min. The fluorescence, then, was normalized to the fluorescence

Biomedical Optics EXPRESS

of negative control giving a value of 'Relative ROS/Superoxide level'. We and others showed that this method is reliable and efficient for evaluating the potency of pro-oxidants and can be used to evaluate the efficacy of antioxidants against oxidative stress in cells [30–34]. CellMask Deep Red plasma membrane stains from Thermo Fisher Scientific have been used for the cell identification during staining of ROS and superoxide content of the cell.

Apoptosis assay

Apoptosis was assessed via annexin V/propidium iodide staining. Cells were treated with different irradiation fluences of laser for 40 min. Phosphatidylserine expression, as an early sign of apoptosis, was determined via fluorescence microscopy analysis by the binding of fluorescein isothiocyanate-labeled annexin V (Sigma-Aldrich); propidium iodide (PI) was used to differentiate necrotic cells. NucRed was used as nuclear staining (Thermo Fisher Scientific). Fluorescence images were recorded using a Bio-Rad MRC-1024 laser scanning confocal microscope (Bio-Rad, Cambridge, MA). ImageJ software (NIH, Bethesda, MD) was used for image processing and fluorescent micrograph quantification. PI and annexin V fluorescence were calculated by normalizing the corrected total cell fluorescence (CTCF) of the full area of interest to average fluorescence of the region. The net average CTCF intensity of a pixel in the region of interest was calculated for each image utilizing a previously described method [35].

Caspase-3 activity assay

As an apoptosis parameter, caspase-3 activation was detected using the caspase-3 inhibitor VAD-FMK conjugated to FITC (FITC-VAD-FMK) as a marker. FITC-VAD-FMK is cell permeable, nontoxic, and irreversibly binds to activated caspases in apoptotic cells. After 40 min post laser irradiation, cells were loaded with FITC-VAD-FMK (Abcam, Cambridge, United Kingdom) according to the manufacturer's instructions. Following the staining, cells were photographed using an epifluorescent microscope IM-2FL (Optika Microscopes, Ponteranica (BG), Italy). Fluorescence intensity was measured using ImageJ software (NIH). As a positive control, cells were treated with 2 μM staurosporine for 3 h.

Quantification of mitochondrial membrane potential

Cells were irradiated with different fluences of laser for 40 min to measure mitochondrial membrane potential (ΔmΦ). After 40 min of irradiation, cells were loaded with 2 μM JC-1 (Thermo Fisher Scientific), a lipophilic cationic fluorescence dye with a dual emission wavelength for 30 min, in order to analyze the depolarization of the ΔmΦ. JC-1 exists either as a green-fluorescent monomer at depolarized membrane potentials or as an orange/red-fluorescent J-aggregate at hyperpolarized membrane potentials. It accumulates in mitochondria depending on ΔmΦ and is present either as monomer or J-aggregate. The JC-1 monomer predominating in depolarized mitochondria emits green fluorescence (~530 nm), whereas the oligomer (J-aggregate) forming in mitochondria with potentials more negative than −140 mV emits red fluorescence (~590 nm) [36, 37]. JC-1 has advantages over other cationic dyes in that it can selectively enter into mitochondria and reversibly change color from red to green as the membrane potential decreases. In healthy cells with high mitochondrial ΔmΦ, JC-1 spontaneously forms complexes known as J-aggregates with intense red fluorescence. On the other hand, in apoptotic or unhealthy cells with low ΔmΦ, JC-1 remains in the monomeric form, which shows only green fluorescence. The ratio of green to red fluorescence is dependent only on the membrane potential but not on other factors such as mitochondrial size, shape, and density, which may influence single-component fluorescence signals [36, 37]. Following staining, cells were analyzed using Bio-Rad MRC-1024 laser scanning confocal microscope (Bio-Rad, Cambridge, MA) for 50 min with 2 min interval between images. ImageJ software (NIH) was used for image processing and quantification.

Biomedical Optics EXPRESS

Detection of mitochondrial reactive oxygen species (Mito-ROS)

Confocal microscopy of cell culture was performed using a Nikon Diaphot 200 microscope (Nikon, Tokyo, Japan) in combination with Bio Rad MRC-1024 confocal laser scanning imaging system (Bio-Rad, Cambridge, MA). Cells were loaded with 5 μM SYTO 13 green (Ex: 490 nm, Em: 516 nm) and 0.5 μM MitoTracker red CM-H_2XRos (Ex: 579 nm, Em: 599 nm) for 15 min at 37°C in the dark, and then irradiated with 1 mW laser for 40 min. ImageJ software (NIH) was used for image processing and fluorescent micrograph quantification. Cellular fluorescence intensity was calculated by normalizing corrected total cell fluorescence (CTCF) of the full area of interest to average single cell fluorescence. The net average CTCF intensity of a pixel in the region of interest was calculated for each image utilizing a previously described method [38].

Confocal microscopy

Nikon Diaphot 200 microscope (Nikon, Tokyo, Japan) in combination with Bio Rad MRC-1024 confocal laser scanning imaging system (Bio-Rad, Cambridge, MA) have been used in this work for the visualization of cells. Eppendorf micromanipulator 5171 (Eppendorf, Wesseling-Berzdorf, Germany), connected to Nikon Diaphot 200 microscope (Nikon, Tokyo, Japan), was used for precise positioning of taper. Fluorescence images were taken with the acquisition software Lasersharp 2000 v5.2 (BioRad, Hercules, CA). ImageJ software (NIH) was used for image processing and quantification.

Statistical analysis

Quantitative results are expressed as mean ± SEM. Results were analyzed by multi-group comparison Fisher's LSD and Newman-Keuls tests. Differences were considered statistically significant at $*P < 0.05$.

3. Results

Laser system characterization

Several studies using low power lasers have reported phototoxic effects of red and near-infrared light on human cells [3, 21, 22]. The major drawback in these studies is distant laser irradiation of biological objects. To investigate the direct laser light effects on living cells, we designed a special laser system allowing direct irradiation of the cell layer in aqueous solutions. Another important reason to use such setup is to provide fundamental basis for development of safe and reliable tools for optogenetics. The success of optogenetics relies on optical tools that can deliver light directly into tissues [39, 40]. Therefore, studies how cells react to direct laser irradiation are very important in optogenetics applications. A scheme of the experimental setup is shown on Fig. 1(A). Positioning of optical tapers in the closest proximity to the cells was performed using an Eppendorf micromanipulator. The divergence of laser radiation was measured first (Fig. 1(C)) and, based on these data, we calculated the dependence of power density from distance for the maximum (1 mW) and minimum (42 μW) laser powers. We selected such laser powers that are most frequently used in biomedical applications [3, 6, 11–13]. More specifically, power levels ranged from 50 to 200 mW are used in LLLT and from 6 to 15 W are applied at high power NIR phototherapy [41]. Specific tissue characteristics as well as laser parameters contribute to variability of biological effects triggered by laser irradiation. The following laser radiation parameters are equally important: wavelength, exposure time, applied energy, focal spot size, energy density and power density [41]. Among these, the exposure time and power density are very crucial parameters when selecting a certain type of cell-laser interaction. The majority of laser medical treatments, such as laser hyperthermia, coagulation, and surgery, involve thermal effects. However, in LLLT non-thermal laser effects are needed. Since power density thermal thresholds for exposure to NIR lasers depend greatly on optical tissue properties such as the coefficients of

Biomedical Optics EXPRESS

reflection, absorption and scattering [41–44], thermal interaction with the laser radiation for most of soft tissues starts at power densities from 50 kW/cm^2 with typical exposure time of several minutes [41–44]. Thus, we selected for our experiments such laser which generates power density below the thermal threshold. At a maximum power of the laser (equal to 1 mW) the power density at a distance of 500 µm was 18.7 kW/cm^2. At minimum power (46 µW), the power density was 0.8 kW/cm^2 at the same distance.

Acute laser damage of Huh7 cell line

To determine the effect of laser irradiation on cellular viability we utilized the LIVE/DEAD Viability/Cytotoxicity Kit which is a quick and easy two-color assay to determine viability of cells [29, 45]. This assay quickly discriminates live from dead cells by simultaneously staining with green-fluorescent calcein-AM to indicate intracellular esterase activity and red-fluorescent ethidium homodimer-1 to indicate loss of plasma membrane integrity [29, 45]. Consistent with previous reports, red laser irradiation did significantly affect the viability of Huh7 within the first 40 min of exposure (Fig. 2(A)). Cell damage from exposure to a laser showed a typical red damage zone (dead cells). Importantly, only continuous red laser irradiation induced acute toxicity of Huh7 cells whereas imaging setup did not affect viability of the control cells (Fig. 2(A), Visualization 1, Visualization 2). At lower power, laser light proved to be less cytotoxic to Huh7 (Fig. 2(B)). In general, the laser beam in aqueous solution due to divergence was about ~40 micron (Fig. 1C). Several cells were irradiated simultaneously. Thus, we carefully considered the non-uniform distribution of laser intensity from the fiber output (Fig. 2(C)). The cells at different area inside the laser spot experienced different irradiation which resulted in non-uniform cellular response (Fig. 2(C)). Indeed, after ~30 min saturation occurred and all irradiated cells at the laser spot had approximately the same cell damage state (Visualization 2). This kinetics experiments were crucial to find out appropriate time frame for further analysis of molecular events triggered by laser irradiation.

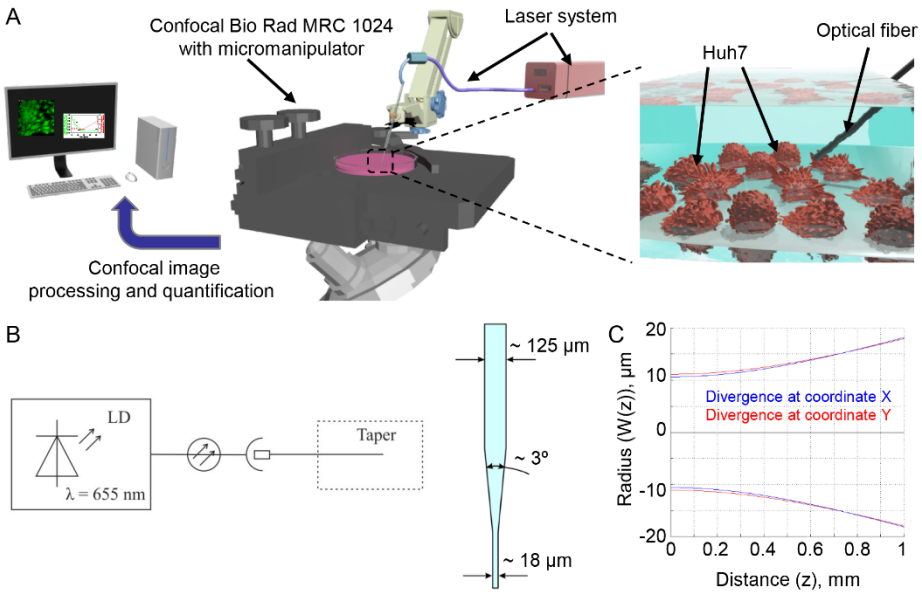

Fig. 1. Characterization of the laser system. (A) Experimental setup. (B) Scheme of the laser system. LD - laser diode. (C) Divergence of laser beam.

Biomedical Optics EXPRESS

Accumulation of ROS drives cytotoxic effects induced by red laser

In the next step, we evaluated ROS generation triggered by laser irradiation using the ROS-sensitive fluorescent dyes. We found that red laser irradiation triggered a dose-dependent ROS production in Huh7 cells (Fig. 3(A-C)). It is clearly shown in Fig. 3(B,C), that laser irradiation induced dose-dependent ROS accumulation in cells with the highest amount of ROS, produced after higher laser power (1 mW) irradiation (Fig. 3(B,C)).

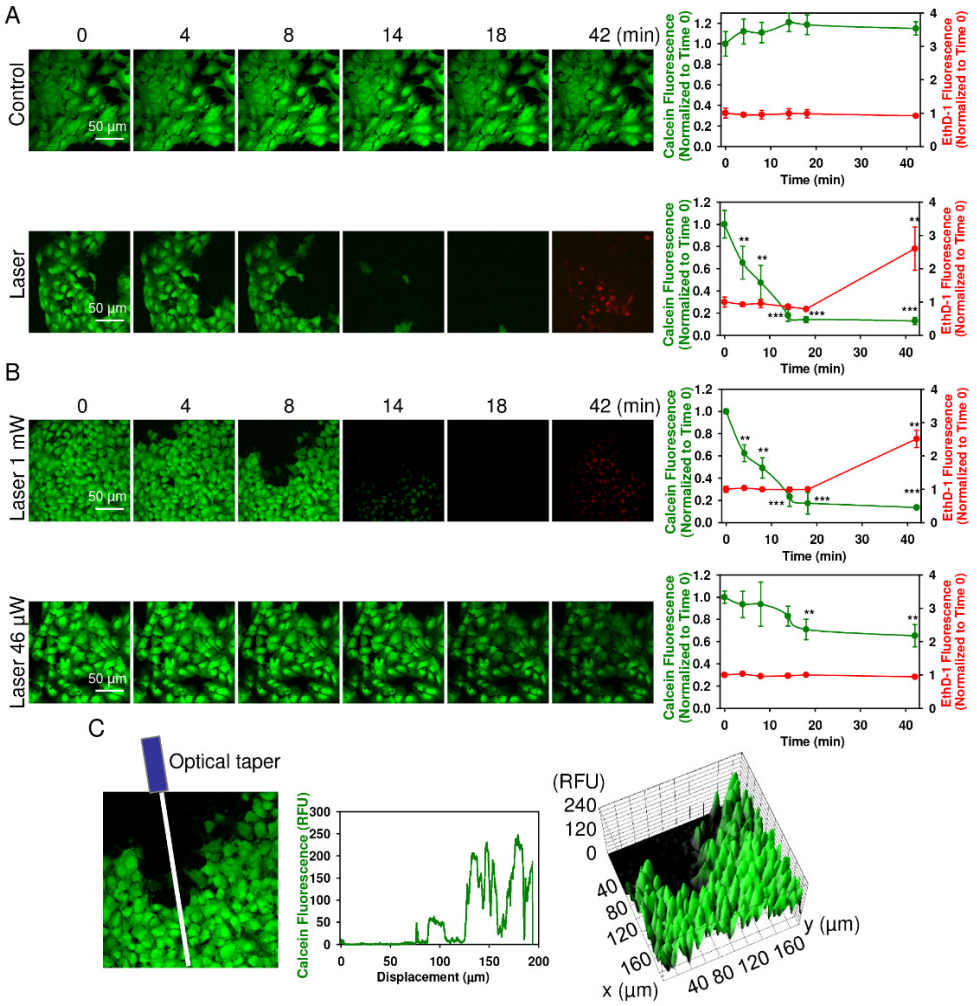

Fig. 2. Laser irradiation induces acute cell death of Huh7 cells. (A) Cell viability was detected by the fluorescent live/dead cell assay kit (Thermo Fisher Scientific). After loading with calcein-AM (green) and ethidium homodimer (red) images were acquired by confocal microscopy from Huh7 cells treated with laser (1 mW). Control cells were untreated. ImageJ software (NIH) was used for image processing and quantification. Fluorescence intensity of both dyes was measured at the respective time points and was normalized to total fluorescence. Data are expressed as means ± SEM (n = 3), t = 0 time point served as control, $^{**}P< 0.01$ $^{***}P< 0.001$. (B) Dose-dependent laser-induced cytotoxicity. Cells were irradiated with different laser fluences and analyzed as in (A). Data are expressed as means ± SEM (n = 3), t = 0 time point served as control, $^{**}P< 0.01$ $^{***}P< 0.001$. (C) Non-uniform cellular response due to the non-uniform distribution of the laser intensity from the fiber output. Line intensity profile and surface intensity plot of cells irradiated with laser (1 mW) as in (B). Graphs show non-uniform calcein-AM fluorescence depending on displacement from optical taper. ImageJ software (NIH) was used for image processing and quantification.

Biomedical Optics EXPRESS

We used two distinct fluorescent probes. One probe used was indicative of cellular production of different ROS types, the other was superoxide (O_2^-) specific. This allowed us to monitor changes in the total ROS level as well as specifically verify the level of superoxide. Indeed, red laser irradiation triggered a dose-dependent accumulation of superoxide as well (Fig. 3(A-C)). To confirm the role for ROS in the induction of acute cell death by laser irradiation, we used the ROS-scavenger *N-acetyl-L-cysteine*. As expected, ROS scavenger was able to antagonize the cytotoxic effects elicited by laser irradiation (1 mW) on Huh7 cells (Fig. 3(D), Visualization 3).

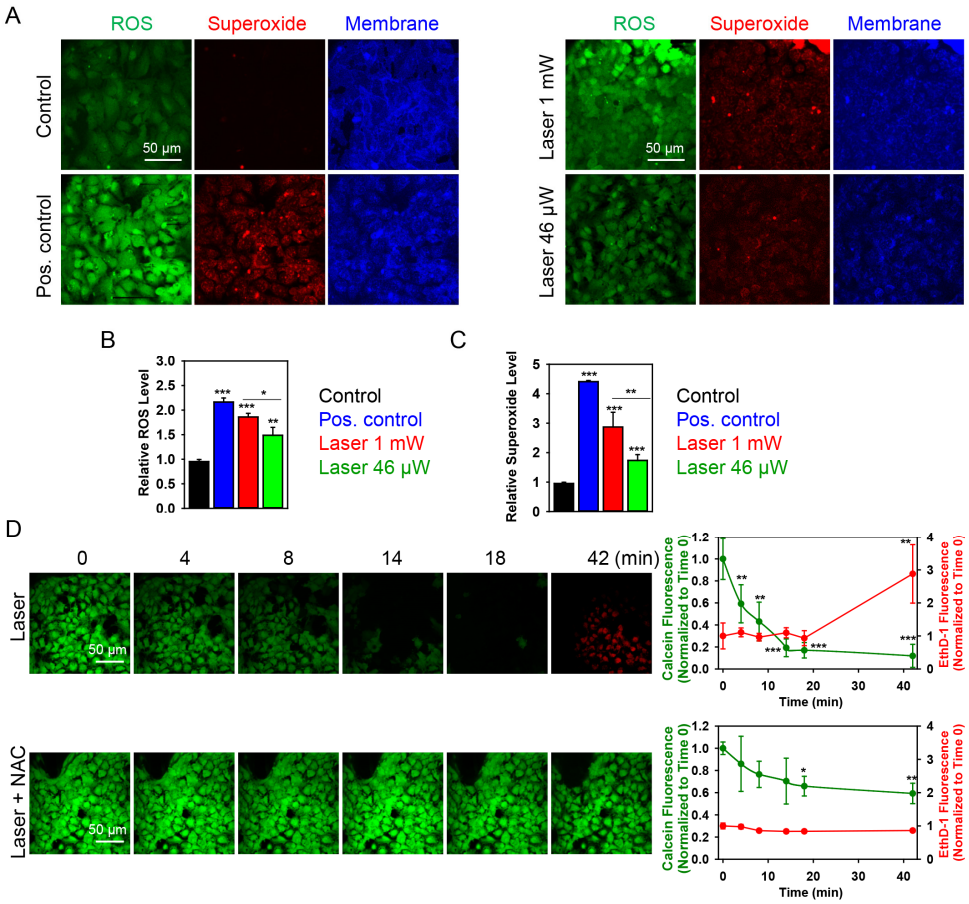

Fig. 3. Dose-dependent ROS induction by laser irradiation. (A) Cells were labeled with the ROS-sensitive fluorescent dyes using the cellular ROS/Superoxide detection kit (Abcam, Cambridge, United Kingdom). Cell membranes were labeled with CellMask. Non-irradiated cells with no chemical treatment served as a negative control (left panel). Non-irradiated cells treated with Pyocyanin (200 µM) were used as a ROS positive control (left panel). Cells irradiated by laser fluences of 1 mW and 46 µW are shown on the right panel. All fluorescence images were acquired by confocal microscopy. (B) Quantitative analysis of relative ROS fluorescence emission intensity from cells treated by laser. ImageJ software (NIH) was used for image processing and quantification. Data are expressed as means ± SEM (n = 3), *P< 0.05 **P< 0.01 ***P< 0.001. (C) Quantitative analysis of relative superoxide fluorescence emission intensity from cells treated by laser. ImageJ software (NIH) was used for image processing and quantification. Data are expressed as means ± SEM (n = 3), *P< 0.05 **P< 0.01 ***P< 0.001. (D) ROS scavenger *N-acetyl-L-cysteine* (NAC) reduces the cytotoxicity induced by laser. Viability of Huh7 cells exposed to the laser for indicated time periods with supplementation of 5 mM NAC was detected by the Thermo Fisher Scientific fluorescent live/dead cell assay kit. Cells were imaged and analyzed as in Fig. 2. Data are expressed as means ± SEM (n = 3), t = 0 time point served as control, *P< 0.05 **P< 0.01 ***P< 0.001.

Biomedical Optics EXPRESS

High dose laser treatment induces necrosis of Huh7 cells

Given the facts that hepatocytes have high number of mitochondria and mitochondria play a crucial role in both necrotic and apoptotic cell death [24, 25], we hypothesized that one could potentially switch between distinct cellular death types using red laser irradiation. Based on these considerations, we explored induction of necrotic cell death at high laser power, i.e. 1 mW.

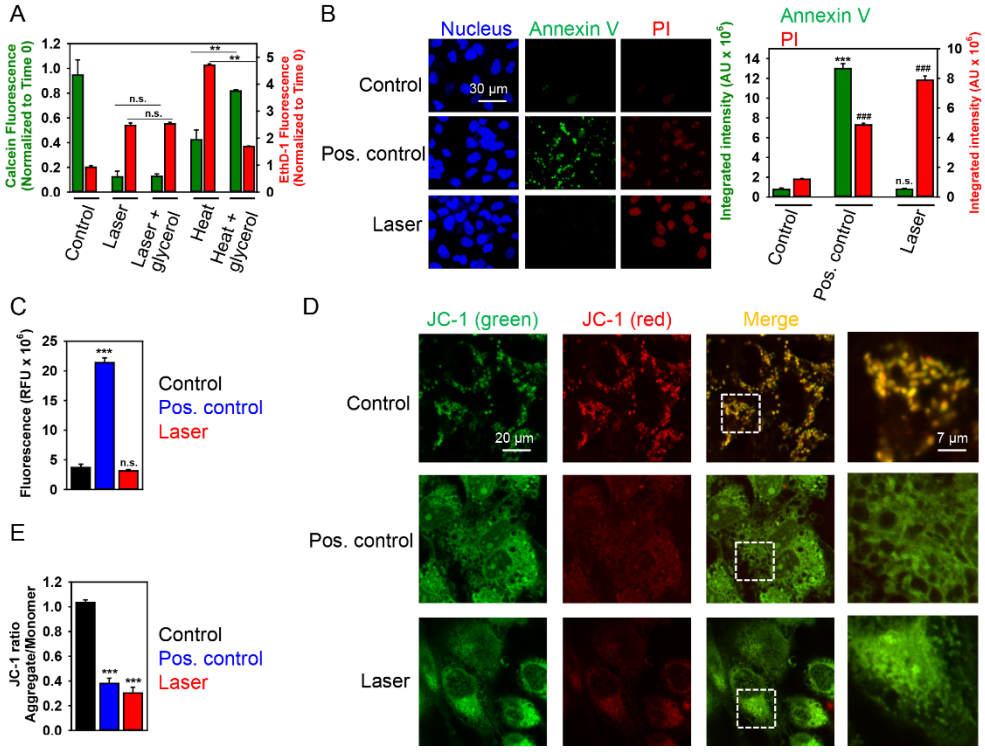

Fig. 4. High dose (1 mW) laser irradiation induces necrotic cell death of Huh7 cells. (A) Cell viability was detected by the Thermo Fisher Scientific fluorescent live/dead cell assay kit. Full growth medium with 1 M glycerol was used as thermoprotective. Cells were imaged and analyzed as in Fig. 2. Data are expressed as means ± SEM (n = 3), $^{**}P< 0.01$. Cells heated for 1 h at 45 °C were used as a positive control. (B) Cells were treated with laser for 40 min and then labeled with NucRed nuclear stain (blue), annexin V (green) and PI (red). Cells treated with 2 μM staurosporine for 3 h served as a positive control. Labeled cells were imaged with fluorescence microscopy. Representative images out of three independent experiments are shown. Annexin V and PI fluorescence intensities were analyzed with ImageJ. Data are expressed as means ± SEM (n = 3), $^{***}P< 0.001$, $^{###}P< 0.001$. (C) Cells were irradiated with laser for 40 min. Further, post-treatment cells were incubated with caspase-3 inhibitor VAD-FMK conjugated to FITC (FITC-VAD-FMK). Following the staining, cells were analyzed using a fluorescent microscope. Fluorescence intensities were analyzed with ImageJ. Data are expressed as means ± SEM (n = 3), $^{***}P< 0.001$. (D) Cells were irradiated with laser for 40 min, then stained with 2 μM JC-1 for 30 min, and analyzed by confocal microscopy. Red fluorescent images of dye aggregates indicate high- ΔmΦ mitochondria. As a positive control, cells were treated with 10% ethanol for 10 min. (E) Quantitative analysis of ΔmΦ imaged in (D). ImageJ software (NIH) was used for image processing and quantification. Data are expressed as means ± SEM (n = 3), $^{***}P< 0.001$.

First of all, we investigated whether high power laser-induced cellular toxicity is driven by possible temperature rise. We supplemented the growth medium of Huh7 cells with 1 M glycerol. Addition of glycerol to medium has been repeatedly shown to protect cells from heat-induced death [46, 47]. Indeed, 1 M glycerol supplementation did not protect from laser-

Biomedical Optics EXPRESS

induced acute cytotoxicity (Fig. 4(A)). Contrary, glycerol was effective in protecting cell death induced by 45 °C heating (Fig. 4(A)). These data suggest that laser-induced acute cytotoxicity is not related to macroscopic heating effects. Our results confirm other previously published studies showing that such laser power (and power density) is unlikely to induce any thermal damage of cells [3, 42]. Furthermore, we measured the absorption coefficient of the physiological buffer system. The absorption coefficient was 0.03598 1/cm at 655 nm wavelength. Due to such small absorption coefficient, one can conclude that the buffer solution is heated to a minimum extent by such laser radiation. Therefore, we can exclude the effect of local heating as potential effector of laser irradiation on living cells.

Exposure of Huh7 cells to high laser power induced no signs of early apoptosis, namely translocation of phosphatidylserine to the outer cell membrane leaflet, as measured by binding of FITC-labeled annexin V (Fig. 4(B)). Instead, a concomitant increase in membrane permeability, as shown by propidium iodide exclusion (Fig. 4(B)), was the predominant effect. Indeed, annexin V-PI double staining suggested that laser irradiation induced either late stage apoptotic or necrotic cell death (Fig. 4(B)). Additionally, to confirm that laser irradiation (1 mW) does not induce apoptosis, we performed caspase-3 activity assay (Fig. 4C). Caspase-3 is an executioner of apoptosis, and its activation constitutes irreversible morphological changes characteristic of the apoptotic process, such as DNA degradation, chromatin condensation, and membrane blebbing [48]. Analysis of caspase-3 activation in cells treated with high fluence laser showed that laser irradiation did not induce apoptotic cell death in Huh7 (Fig. 4(C)). It is worth noting here that treatment with staurosporine (a well-known apoptosis inducing compound) resulted in caspase-3 activation (Fig. 4(C)) and translocation of phosphatidylserine to the outer cell membrane leaflet (Fig. 4(B)).

Mitochondria have been identified as one of major sources of cellular ROS generation [49, 50]. Moreover, the superoxide anion is generated as a by-product of mitochondrial oxidative phosphorylation [51]. The generation and accumulation of superoxide is primarily associated with cellular toxicity and mitochondrial dysfunction [51, 52]. Furthermore, number of studies point toward mitochondria as a central organelle which activity is affected by red laser light irradiation and that mitochondria damage is the main cause of laser-induced cytotoxicity [3, 9, 20, 23]. The induction of mitochondrial membrane surface charge dissipation and corresponding change of mitochondrial membrane potential ($\Delta m\Phi$) is sufficient to trigger apoptosis or necrosis [50, 53]. Thus we used the fluorescent dye JC-1 to investigate whether laser irradiation (1 mW) may perturb mitochondrial function. JC-1 represents a cationic dye that exhibits a potential-dependent accumulation in mitochondria, which can be monitored by a shift in fluorescence emission from green to red [54]. Untreated control cells that were stained with the fluorescent dye JC-1 exhibited numerous, brightly stained mitochondria that emitted red-orange fluorescence (Fig. 4(D,E)), representing J aggregates that accumulate at normally hyperpolarized membrane potential. After laser treatment, the J aggregates in Huh7 cells were barely visible, indicating complete collapse of $\Delta m\Phi$. Meanwhile, some green fluorescence of monomers appeared in the cytoplasm, representing the depolarized mitochondria (Fig. 4(D,E)). Interestingly, high dose of ethanol - a known inducer of rapid accidental necrosis in hepatocytes [55, 56] - triggered much more severe and rapid mitochondria disintegration than laser irradiation (Fig. 4(D)). These data suggest that signaling cascades triggered by ethanol and laser may be grossly different. In particular, 1 mW laser irradiation may induce specific type of necrosis.

Low dose laser treatment results in apoptosis of Huh7 cells

To further validate possibility of triggering different biochemical cascades by the same laser light irradiation, we focused on cellular responses triggered by low power laser irradiation, i.e. 46 μW. Analysis of Huh7 treated with low power laser confirmed expression of annexin V on cellular membrane prior to the increase of the cell membrane permeability (Fig. 5(A)). Additionally, analysis of caspase 3 activation in cells treated with 46 μW laser showed that,

Biomedical Optics EXPRESS

indeed, lower laser irradiation dose induced apoptotic cell death, which was evident already 30 min after exposure to the laser (Fig. 5(B)). Importantly, lower laser irradiation dose resulted in gradual dissipation of mitochondrial membrane potential which was significantly lower in comparison with high laser irradiation dose, as assed by JC-1 staining (Fig. 5(C)).

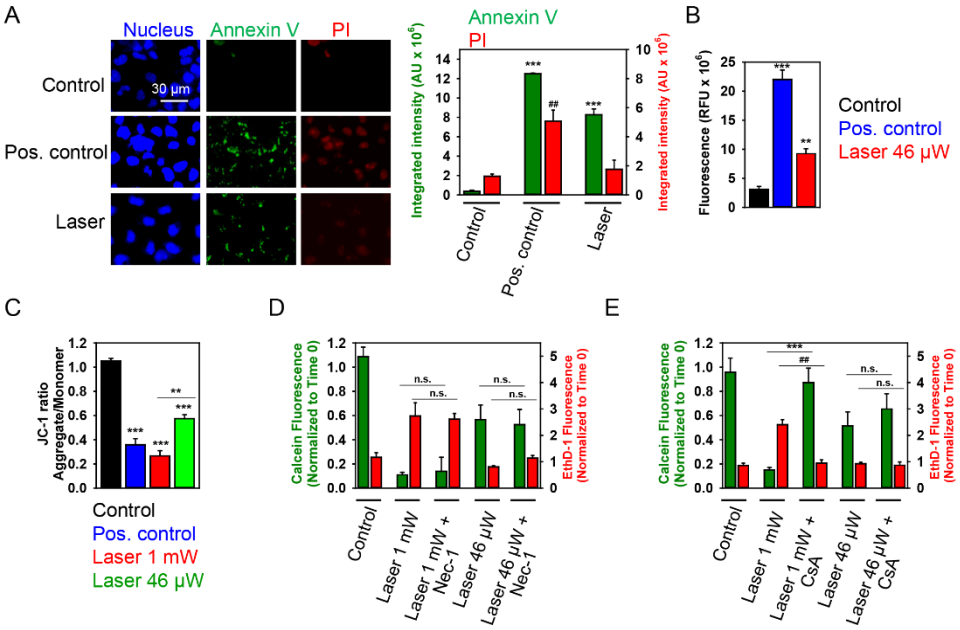

Fig. 5. Low dose laser irradiation induces apoptotic cell death of Huh7 cells. (A) Cells were treated with low dose (46 µW) laser irradiation for 40 min and then labeled with NucRed nuclear stain (blue), annexin V (green) and PI (red). Cells treated with 2 µM staurosporine for 3 h served as a positive control. Labeled cells were imaged with fluorescence microscopy. Representative images out of three independent experiments are shown. Annexin V and PI fluorescence intensities were analyzed with ImageJ. Data are expressed as means ± SEM (n = 3), ***P< 0.001, $^{\#\#}P$< 0.01. (B) Cells were treated with low dose (46 µW) laser irradiation for 40 min and then incubated with caspase-3 inhibitor VAD-FMK conjugated to FITC (FITC-VAD-FMK). Following the staining, cells were analyzed using a fluorescent microscope. Fluorescence intensities were analyzed with ImageJ. Data are expressed as means ± SEM (n = 3), **P< 0.01 ***P< 0.001. (C) Cells were treated with low dose (46 µW) laser for 40 min then stained with 2 µM JC-1 for 30 min and then analyzed by confocal microscopy. As a positive control, cells were treated with 10% ethanol for 10 min. ImageJ software (NIH) was used for image processing and quantification. Data are expressed as means ± SEM (n = 3), **P< 0.01 ***P< 0.001. (D) Viability of Huh7 cells exposed to the laser light with supplementation of 10 µM Nec-1 (1 h pre-treatment with Nec-1 followed by 40 min laser irradiation) was detected by the Thermo Fisher Scientific fluorescent live/dead cell assay kit. Cells were imaged and analyzed as in Fig. 2. Data are expressed as means ± SEM (n = 3). (E) Viability of cells exposed to the laser light with supplementation of 20 µM CsA (1 h pre-treatment with Cs-A followed by 40 min laser irradiation) was detected as in (D). Cells were imaged and analyzed as in Fig. 2. Data are expressed as means ± SEM (n = 3), $^{\#\#}P$< 0.01 ***P< 0.001.

As a matter of fact, ROS accumulation and ΔmΦ dissipation have been implicated in biochemically distinct death pathways, e.g. apoptosis, necrosis, necroptosis [25, 57, 58]. Furthermore, there is a signaling crosstalk between these cascades of death pathways via ROS [27, 58]. Indeed, viability analysis of cells supplemented with necrostatin-1 (Nec-1, a well-known inhibitor of necroptosis [59]) revealed, that neither low dose, nor high dose laser irradiation-induced cytotoxicity was affected by Nec-1 (Fig. 5(D)). On the other hand, high laser irradiation dose induced higher depolarization of the mitochondrial membrane (Fig. 5(C)) and superoxide accumulation (Fig. 3(A,C)) in comparison with low dose. High laser

Biomedical Optics EXPRESS

irradiation-induced cytotoxicity was inhibited by specific pharmacological inhibitor cyclosporin A (CsA) of cyclophilin D (CypD), indicating that high laser irradiation triggers CypD-related necrosis via the mitochondrial permeability transition (mPT) (Fig. 5(E)). Further, to validate our findings that high laser irradiation triggers CypD-related necrosis, we analyzed inhibitory effects of CsA on collapse of ΔmΦ triggered by laser irradiation. Indeed, pretreatment of Huh7 cells with 10 µM CsA significantly inhibited mitochondria damage induced by the laser irradiation (Fig. 6(A)). Additionally, CsA blocked generation of mitochondrial ROS triggered by laser treatment (Fig. 6(B)). Moreover, to confirm the role for ROS in the induction of mitochondrial damage by laser irradiation, we used the ROS-scavenger *N-acetyl-L-cysteine*. ROS scavenger was able to antagonize the mitochondrial damage elicited by the laser irradiation (1 mW) on Huh7 cells (Fig. 6(C)). All these findings confirmed that high laser irradiation triggers CypD-related necrosis via the mitochondrial permeability transition.

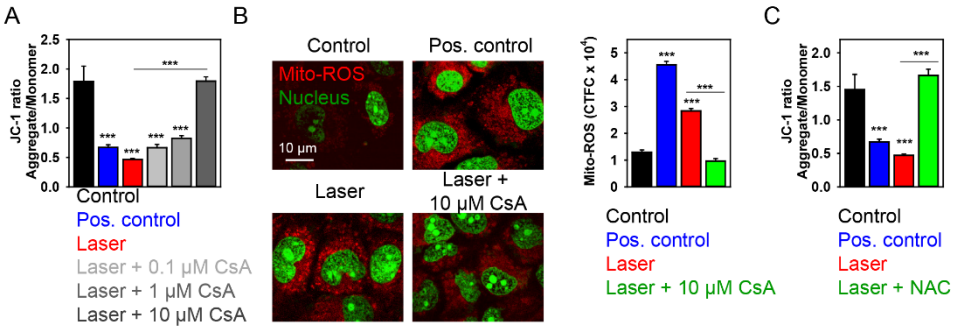

Fig. 6. Cyclosporin A inhibits depolarization of mitochondrial membrane potential exerted by 1 mW laser irradiation. (A) Cells were irradiated with laser for 40 min, then stained with 2 µM JC-1 for 30 min, and analyzed by confocal microscopy. Red fluorescent images of dye aggregates indicate high- ΔmΦ mitochondria. Cells were preincubated with 0.1, 1, 10 µM CsA before treatment with laser. As a positive control, cells were treated with 10% ethanol for 10 min. Quantitative analysis of ΔmΦ was performed by ImageJ software (NIH). Data are expressed as means ± SEM (n = 5), ***P< 0.001. (B) Cultures were co-loaded with SYTO 13 (green) and MitoTracker red CM-H_2XRos (red) and confocal images (1000x) obtained after 1 mW laser irradiation. Cells were preincubated with 10 µM CsA before treatment with laser. Representative images out of three independent experiments are shown. Non-irradiated cells treated with Pyocyanin (200 µM) were used as a ROS positive control. Mito-ROS fluorescence intensities were analyzed with ImageJ. Data are expressed as means ± SEM (n = 3), ***P< 0.001. (C) ROS scavenger *N-acetyl-L-cysteine* (NAC) reduces the mitochondrial damage induced by laser. Mitochondrial damage of cells exposed to the laser with supplementation of 5 mM NAC was performed using JC-1 assay as in (A). Data are expressed as means ± SEM (n = 3), ***P< 0.001.

Low dose laser treatment triggers nuclear accumulation of superoxide

Further, we elucidated possible reasons for triggering different specific types of cell death by different doses of the same wavelength of laser irradiation. It has been shown that formation of specific ROS can lead to different molecular cell death mechanisms (necrosis and apoptosis) and that ROS might dictate different cellular consequences depending on their overall concentration at steady-state levels and on their site of generation [60, 61]. Moreover, a recent study shows that oxidants and their targets might be spatially confined within the cell [62]. Based on these considerations, we explored the effect of different laser doses on sub-cellular localization of ROS. Indeed, Nuclear accumulation of the superoxide anion triggered by low laser dose was significantly higher in comparison with high dose laser irradiation and pyocyanin treatment resulted in the highest superoxide accumulation in the nucleus (Fig. 7(A,B)). Since accumulated in cellular nucleus superoxide is responsible for DNA double-strand breaks [63] and the literature evidence suggests that DNA double-strand breaks results

Biomedical Optics EXPRESS

in execution of apoptosis whereas DNA base damage induces necrosis [64], it becomes understandable why low laser dose triggers apoptosis whereas high dose results in necrosis.

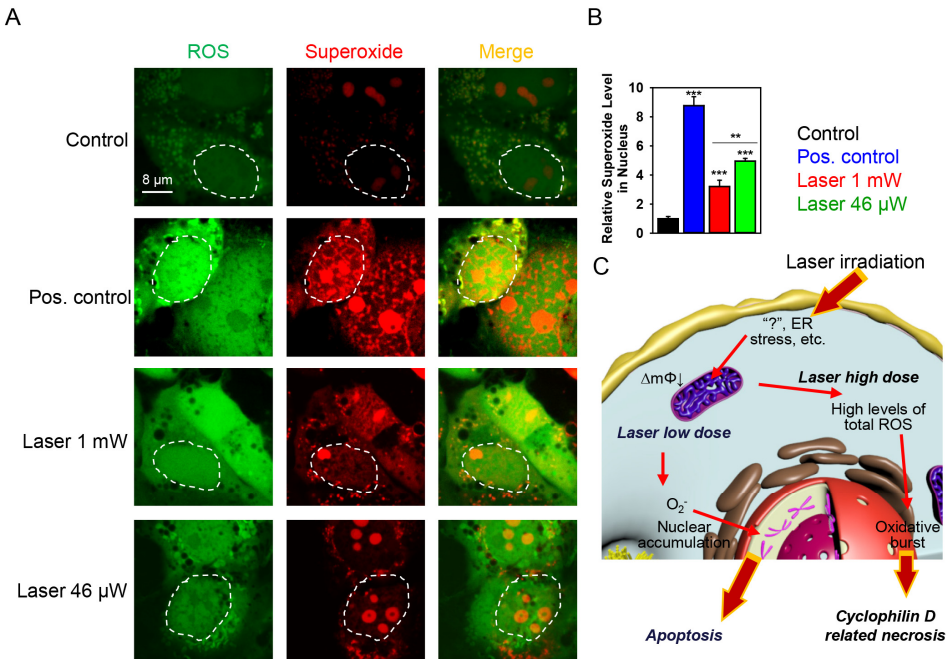

Fig. 7. Low dose laser irradiation induces nuclear accumulation of superoxide. (A) Cells were labeled with the ROS-sensitive fluorescent dyes using the cellular ROS/Superoxide detection kit (Abcam, Cambridge, United Kingdom) and then treated by different laser fluences. The fluorescence images were acquired by confocal microscopy. Non-irradiated cells with no chemical treatment served as control. Pyocyanin (200 μM) treatment was used in the non-irradiated cells representing the ROS + positive control. (B) Quantitative analysis of relative superoxide fluorescence emission intensity from cells treated by laser. ImageJ software (NIH) was used for image processing and quantification. Data are expressed as means ± SEM (n = 3), $^{**}P< 0.01$ $^{***}P< 0.001$. (C) Scheme of district biochemical signaling activation in cells after stimulation with different laser doses. ΔmΦ – mitochondrial membrane potential.

4. Discussion

Nowadays Low Level Light/Laser Therapy utilizing low-power red lasers is becoming more and more popular. However, clinical applications of such therapy are restrained due to the lack of knowledge about the molecular mechanisms of laser-living cell interactions. Red laser light irradiation has been known to induce ROS production and phototoxicity in different cell types [3, 9, 20, 23]. Also some photobiomodulation effects of LLLT are known using red and NIR light at 600–1,000 nm with intensity of 3–90 mW/cm^2 [30]. Epidermal stem cells in the hair follicle bulge were shown to promote hair growth by LLLT treatment [34]. Photobiomodulation has been found efficacious for wound healing, tissue repair and anti-inflammatory therapy [3]. However, results from clinical trials have been mixed, underlying mechanisms of LLLT and photobiomodulation are not well understood and therefore adoption of photobiomodulation has been controversial [30]. Additionally, a large number of parameters such as the wavelength, fluence, power density, pulse structure, and timing of the applied light must be chosen for each treatment. Thus, all the aforementioned limitations make direct head-to-head comparisons of LLLT and photobiomodulation regarding efficacy and safety particularly challenging.

In light of previous studies demonstrating red laser induced cell apoptosis via the mitochondria/caspase-3 signaling pathway [9, 20, 65] and taking into account fact that

Biomedical Optics EXPRESS

mitochondria plays crucial role in both necrotic and apoptotic cell death [24, 25], we hypothesized that one could modulate mitochondria activity by laser triggering distinct biochemical cascades. This study was motivated by the lack of a precise molecular pathway of phototoxicity data for the use of red lasers. Here we show that both high and low doses of laser irradiation produce intracellular ROS, accumulation of which leads to cell death. Indeed, ROS are emerging as key effectors in signal transduction [66]. The role of ROS is especially evident in pathways leading to apoptosis, elicited in response to certain stress stimuli. We found consistently with previous reports [9, 20] that low dose of laser irradiation induces apoptosis (Fig. 5(A-C)). Contrary, high laser dose treatment results in CypD-related necrosis via the mPT (Fig. 4, Fig. 5(D,E) and Fig. 6). Despite that addition of pharmacological inhibitor cyclosporin A inhibited necrosis induced by high laser dose, CsA was not effective in inhibition of apoptosis triggered by low lase dose (Fig. 5(E) and Fig. 6). Pretreatment of Huh7 cells with 10 μM CsA significantly inhibited mitochondria damage and generation of mitochondrial ROS triggered by the laser treatment (Fig. 6(A,B)). Additionally, we confirmed the role of ROS in mitochondrial damage due to the laser irradiation (Fig. 6(C)). Our observation is in line with previously published results showing that CsA failed to prevented apoptotic cell death induced by red laser [9]. Furthermore, mechanisms that block mPT, like CsA or knocking out cyclophilin-D, reduce mostly necrosis and, in some cases (not all cell types are responsive), also suppress apoptosis [67, 68]. On the other hand, the defining event in apoptosis is mitochondrial outer membrane permeabilization (MOMP), allowing apoptogen release, whereas the triggering event in necrosis is early opening of the mPT [69, 70]. Interestingly, recent study showed that the transient opening of mPT may help to scavenge mitochondrial ROS to protect cells in the case of moderate and short stimulation by femtosecond laser [71]. Another study suggested that short-duration femtosecond-laser stimulation can induce restorable fragmentation or swelling of any targeted mitochondria [72]. Additionally, mitochondrial oxidative stress triggered by high-fluence low-power laser irradiation may affect mitochondrial dynamics [73]. Of note, in our study we focused on cellular effects induced by continuous laser rather than pulsed. Taking together, those results suggest the mitochondrial and molecular response to laser irradiation is quite complex. Thus, it is no surprise that different laser doses trigger distinct biochemical pathways of cell death. Future studies are needed to reveal in details molecular mechanisms of laser action on living cells.

On the basis of our results, we propose the following tentative biochemical mechanisms of laser irradiation action on living cells (Fig. 7(C)). Laser treatment results in ROS accumulation in cells which leads to oxidative stress. Such oxidative stress results in dissipation of mitochondrial membrane potential. Depending on dose of laser irradiation mitochondrial damage is either accompanied by triggering of apoptosis or results in necrotic cell death (Fig. 7(C)). Mitochondria have a biological fluorophore, cytochrome c oxidase, and once affected by laser light, it produces ROS and induces mitochondrial impairment [9, 20, 74, 75]. Moreover, it has been demonstrated that irradiation at 632.8 nm affects redox state of cytochrome c oxidase [76]. Thus, it is not surprising that red laser light targets mitochondria activity. We propose here a tentative explanation and the model of the observed effects. In fact, using pharmacological and biochemical approaches, our results identify mitochondria as one of cellular ‘effectors’ of laser irradiation. Deciphering of exact mechanisms of laser action on living cells is inherently very complex and requires further experiments and investigation. Indeed, the identification of the intracellular ‘sensor’ of laser irradiation is a complex task, which is currently under investigation.

Importantly, upon low dose laser irradiation there is significantly higher accumulation of the superoxide anion in the cell nucleus (Fig. 7(A,B)) in comparison with high dose irradiation. As far as nuclear superoxide accumulation is responsible for DNA double-strand breaks [63] and such breaks results in execution of apoptosis [64], it is becoming evident why different dose of laser irradiation trigger distinct biochemical pathways of cell death.

Biomedical Optics EXPRESS

Moreover, in recent years it has become increasingly clear that oxidative and reductive modifications are confined in a spatio-temporal manner [77]. Therefore, different doses of laser irradiation result in different intracellular ROS compartmentalization which in turn may lead to initiation of distinct biochemical cascades.

5. Conclusions

In summary, we have demonstrated that cell treatment with different doses of laser irradiation led to activation of distinct biochemical signaling that triggers cell death pathways. Therefore, cytotoxicity of red laser-based therapies should be carefully considered in clinical practice. Furthermore, we showed that ROS scavenger *N-acetyl-L-cysteine* reduced cytotoxicity caused by ROS production induced by laser irradiation. This indicates that dietary supplementation with antioxidants might be a suitable strategy to reduce laser light-induced oxidative damage.

Funding

Academy of Sciences of the Czech Republic (J.E. Purkyne fellowship); MH CZ - DRO Institute for Clinical and Experimental Medicine (IKEM, IN 00023001); MEYS of the Czech Republic (LO1309) Ministry of Education and Science of Russian Federation (goszadanie no 8.3134.2017/4.6).

Disclosures

The authors declare that there are no conflicts of interest related to this article.